EuroGNC Navigation Guidance Control CEAS Bristol, UK June 11th-13th 2024
University of BRISTOL ROYAL AERONAUTICAL SOCIETY AIAA

Automated Mission Generation and Dispatching for BVLOS Drone Operations

Tobias Islam Chief Engineer, RWTH Aachen University, Institute for Flight System Dynamics, 52062, Aachen, Germany. islam@fsd.rwth-aachen.de

Sebastian Seitz Chief Engineer, RWTH Aachen University, Institute for Flight System Dynamics, 52062, Aachen, Germany. seitz@fsd.rwth-aachen.de

Dieter Moormann Head of Institute, RWTH Aachen University, Institute for Flight System Dynamics, 52062, Aachen, Germany. moormann@fsd.rwth-aachen.de

ABSTRACT

An efficient mission generation and dispatching method was developed for a highly automated Beyond Visual Line of Sight (BVLOS) drone flight campaign conducted in Saxony, Germany, involving the aerial photography of numerous agricultural fields. The methodology incorporates a post-smoothed A* algorithm for path planning to ensure time-efficient routes of up to four tilt-wing aircraft flying in parallel, while taking into account aircraft specific range limitations and velocity constraints imposed by the flight geography. The dispatching method is based on a Vehicle Routing Problem (VRP) formulation and includes the identification of suitable take-off and landing regions within the flight geography. The proposed system provides a solution for efficient mission planning, even in flight geographies with variable speed limits, thereby improving the overall operational effectiveness of BVLOS drone missions.

Keywords: Flight Path Generation; BVLOS Drone Operations; A-Star

Nomenclature

n_d	=	number of depots
p_i	=	Position of Node i
R	=	Effective flight range
V_A	=	Aerodynamic velocity
V_W	=	Wind speed
$\overline{V}_A$	=	Mean aerodynamic velocity
$w_{i,j}$	=	Edge cost between Node i and j
x	=	Solution vector
D	=	Distance matrix
$f(x)$	=	Objective function
$\|p_i - p_j\|_2$	=	Euclidean distance between points i and j

1 Introduction

Unmanned Aerial Vehicles (UAVs) have witnessed a remarkable proliferation in various fields, including agriculture and mining [1], support of rescue missions [2], transportation of medical supplies [3], and inspection of infrastructure [4, 5]. The use of UAVs in these applications has been greatly facilitated by technological advances, automation, and the development of beyond visual line of sight (BVLOS) capabilities. In recent years, BVLOS operations have gained considerable attention in the field of environmental monitoring [6, 7]. These operations have the potential to revolutionize the monitoring and management of agricultural landscapes by providing timely and high-resolution aerial imagery that is crucial for optimizing crop yields, resource allocation, and decision-making processes [8].

However, conducting BVLOS drone flights over large regions presents complex challenges related to mission planning, path optimization, and resource utilization [9]. Agricultural fields are often vast, covering many square kilometers, and the need for timely data collection over these expansive areas presents logistical challenges. These operations must account for factors such as varying field sizes, terrain types, and the location of potential obstructions such as buildings, power lines, and natural obstacles. In addition, regions with non-uniform velocity limits must be considered, which is crucial in the flight path generation process to ensure efficient flight missions.

The ability to optimize the total duration of drone missions ensures timely data collection, minimizes operational costs, and maximizes resource utilization. This is particularly important in scenarios where multiple drones are involved in parallel flights, as was the case in our drone flight campaign in Saxony, Germany [8].

The UAVs used in the context of this paper are tilt-wing aircraft [8, 10], which are hybrid UAVs capable of switching between vertical takeoff and landing (VTOL) and fixed-wing flight modes. This versatility allows them to cover greater distances efficiently, but it also introduces distinct range and flight mechanical constraints that must be carefully considered in mission planning [11].

This paper focuses on addressing these challenges in the context of a highly automated BVLOS UAV flight campaign conducted in Saxony, Germany. The flight campaign was conducted in July 2023 with a parallel operation of up to four UAVs and a total flight distance of more than 10000 km. The primary objective of this campaign was the aerial photography of numerous agricultural fields, which required the efficient generation and dispatch of flight missions. Fig. 1 shows an overview of the numerous points of interest of the entire mission. To achieve this goal, we have developed a method that uses a post-smoothed variant of the well-known A* algorithm for path planning, followed by a variant of the Vehicle Routing Problem (VRP) to generate complete flight missions for the UAVs. This approach ensures the time-efficient routing of up to four tilt-wing aircraft flying in parallel, taking into account aircraft specific range limitations and velocity constraints imposed by the flight geography.

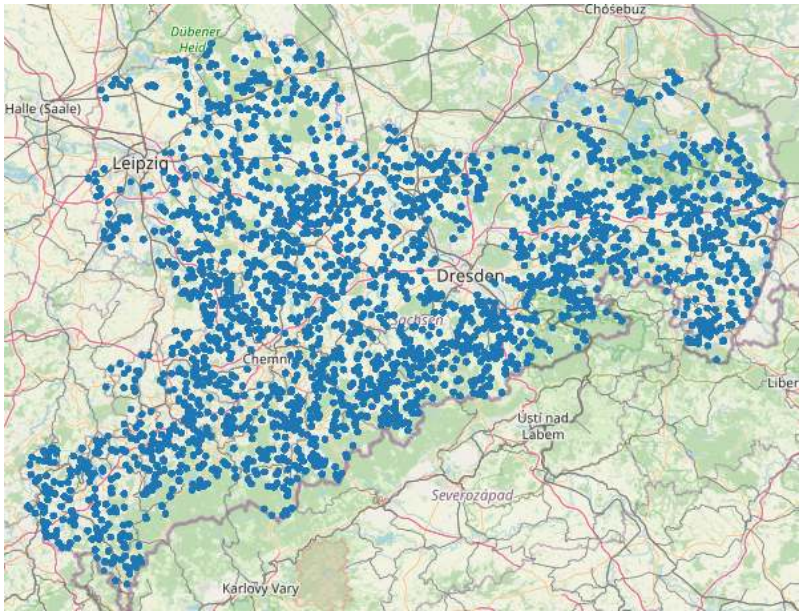

Fig. 1 Points of Interest of the flight campaign. Map data © OpenStreetMap.

In the following chapters, we will discuss the technical details of our methodology, including the path-finding algorithm, the method for identifying suitable take-off and landing regions within the flight geography, and the formulation of the Vehicle Routing Problem (VRP) for mission routing. Finally, we will present results from the mission generation for the BVLOS flight campaign.

2 Representation of the Flight Geometry

The flight geography covers an area of 13.906 km^2 (75% of the total area of Saxony) and consists of three different inertial velocity restrictions. Obstacles such as wind turbines, geofence zones, power lines, and restricted airspace are embedded as holes in the polygons defining the flight geography. The complete flight geography is described by 1,855 polygons with a total of 2,846,559 vertices. Figure 2 shows a section of the flight geography of the flight campaign.

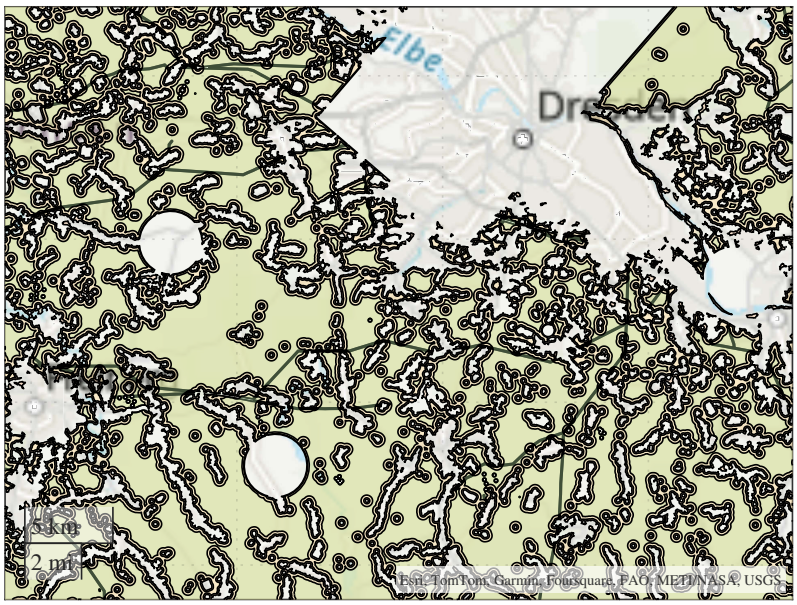

Fig. 2 Exemplary section of the flight campaign's flight geography

To reduce the complexity of the flight geography, we applied a spatial discretization of the given flight geography. The entire area is transformed into a uniform grid with a grid point spacing of 50 m. The spacing is chosen to minimize the overall grid size while ensuring that even the smallest obstacles (e.g., wind turbines) are reliably represented in the grid. Each grid node also contains the corresponding inertial velocity constraint at the node's position in the flight geography. Fig. 3 shows an example of the discretization method.

In the operating permit of the flight campaign[12], three different flight areas were specified, each with different height and velocity constraints. The green, yellow, and orange colors indicate regions with different inertial velocity limits. This method increases the memory required to hold the representation of the flight geography, but significantly reduces the computational complexity to determine if a given location is outside the valid flight geography. It also simplifies obtaining the velocity limit at that location, since the model can simply be stored in a two-dimensional array and locations can be indexed into the array without any complex geometric computations on the polygons.

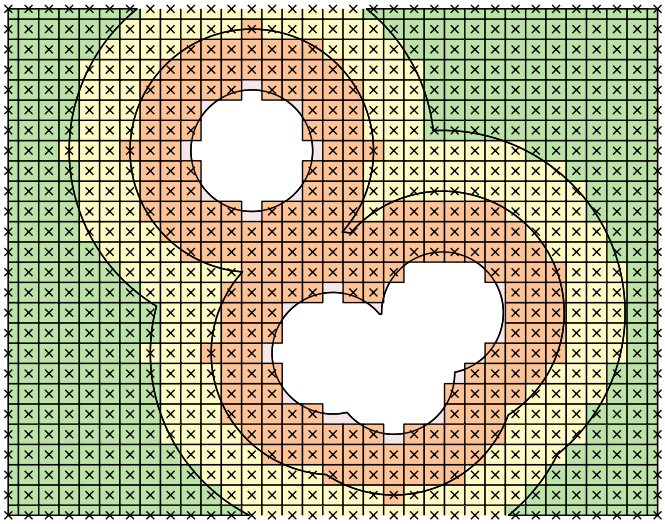

Fig. 3 Discretization of the flight geography

The resulting grid contains approximately 12 million grid points and was pre-computed after obtaining the operational permit, which was tied to the flight geography application, but without knowledge of the target agricultural points of interest. In order to use an efficient path-finding algorithm, an implicit graph is formulated using the grid nodes.

Each grid node represents a node in the graph and is connected to its eight neighbors. The edge cost describes the average energy consumption of the UAV to move between the nodes, considering the inertial velocity constraint imposed by the flight geography and an assumed wind. Since the wind is not known in advance, a conservative assumption is made to avoid underestimating the energy consumption and thus to avoid generating flight paths that the UAVs are unable to fly. The edge cost between two nodes is given by Eq. 1:

$$w_{ij} = E\left(\overline{V}_A\right) |p_i - p_j|_2 \tag{1}$$

p_i and p_j denote the position of the corresponding nodes. The specific energy consumption $E\,(V)$ is a UAV specific function that relates the stationary aerodynamic flight speeds to the energy consumption per distance flown. The specific energy consumption is expressed in units [J / m]. $\overline{V}_A$ is a conservative approximation of the maximum mean aerodynamic velocity given an assumed wind speed and a maximum inertial velocity constraint (Eq. 2).

$$\overline{V}_A = \frac{2}{\frac{1}{V_{A,max}+V_W} + \frac{1}{V_{A,max}-V_W}} \tag{2}$$

Note that edge costs are not explicitly computed and stored for all nodes because there are only a small number of different possible results:

Due to the connectivity of the nodes and the equal horizontal and vertical spacing, there are two distinct distances, 50 m distance between horizontally or vertically adjacent nodes and 70.71 m distance for diagonally adjacent nodes. In addition, depending on the number of different inertial velocity limits, the number of possible transitions between these different limits when going from one node to a neighboring node is simply the number of combinations with repetition:

$$\left(\binom{n}{2}\right) = \binom{n+2-1}{2} = \binom{n+1}{2} = \frac{(n+1)!}{2(n-1)!} = \frac{n(n+1)}{2} \tag{3}$$

where n is the number of different inertial velocity limits. In our case, we have a flight geography with three different values, resulting in 6 possible transitions and, considering two different distances, only 12 possible edge cost values for the whole flight geography. These variants are precomputed and can be easily identified during the path-finding algorithm, so there is no need to recompute the same values each time a node is explored during path-finding, while also reducing the memory consumption of the graph representation.

3 Path-finding Algorithm

In this paper we use a post-smoothed variant of the A-Star algorithm [13]. This method involves two steps: first, the shortest path between a given start and end point on the graph defined in the previous section is found using the standard A-Star algorithm. In a second step, this path is smoothed using the discrete model of flight geography.

The graph nodes are evenly spaced 50 meters apart in the north-south and east-west directions. The destination POIs are not guaranteed to coincide with the grid nodes of the graph. Therefore, the target POIs are linked to the (up to) eight neighboring nodes in the graph (see Fig. 4).

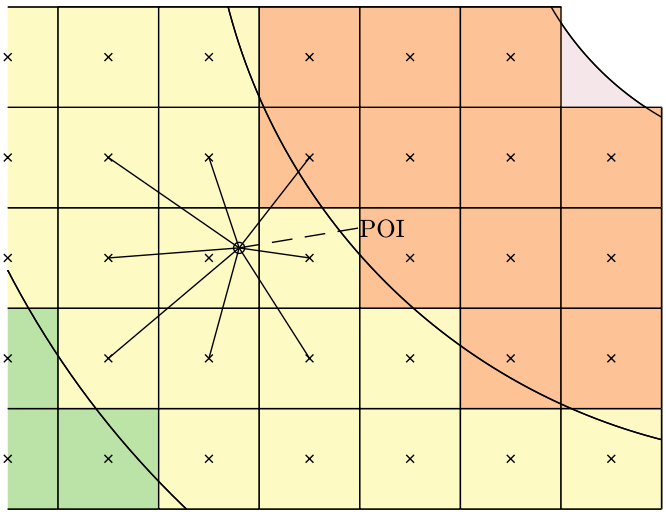

Fig. 4 Linking of POIs in the grid

The heuristic $h(p_i)$, shown in Eq. 4 and used in the A-Star algorithm, is simply given by optimal specific energy consumption per meter times the Euclidean distance between the position of the current node and the position of the target node.

$$h(p_i) = E\left(\overline{V}_{A,opt}\right)|p_{goal} - p_i|_2 \tag{4}$$

Since the range of the UAVs is limited by the energy of the batteries, we introduced a constraint on the maximum energy consumption during the path-finding process to stop the search even if there is theoretically a path between the start and target nodes.

Fig. 5 shows an example result of the A-Star path-finding algorithm. Obviously, the resulting path is not well suited because it has many unnecessary turns resulting from the underlying graph representation.

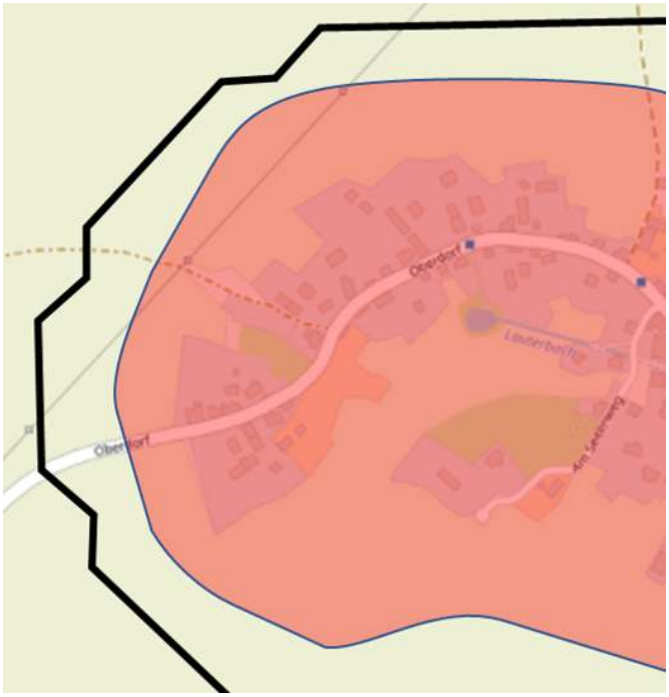

Fig. 5 Example of the non-smoothed A-Star path-finding algorithm

The second step of the method attempts to smooth the resulting path and remove points along it. This minimizes the number of points defining the path, while the algorithm ensures that the smoothed path remains within the flight geography. It also ensures that the path segments that transition from one inertial velocity limit boundary to another do not change. These transition points are important to ensure the shortest path property of the flight path.

To verify if a path segment falls within the flight geography, the Bresenham's line algorithm[14] can be employed. However, this approach, while swift, does not guarantee to find all intersected cells. This meant it might miss crucial intersections with the intricate polygons constituting the original flight geography. To address this, we utilized a modified algorithm, known as the Bresenham-based supercover line algorithm[15]. Unlike its predecessor, this enhanced version guarantees the inclusion of all intersected squares, ensuring comprehensive coverage for accurate evaluation. Fig. 6 shows an example of the resulting set of discrete points to approximate a given continuous line defined by its endpoints. This avoids the complex mathematical operations that would be involved in checking the line segments for intersections with the many polygons of the original flight geography.

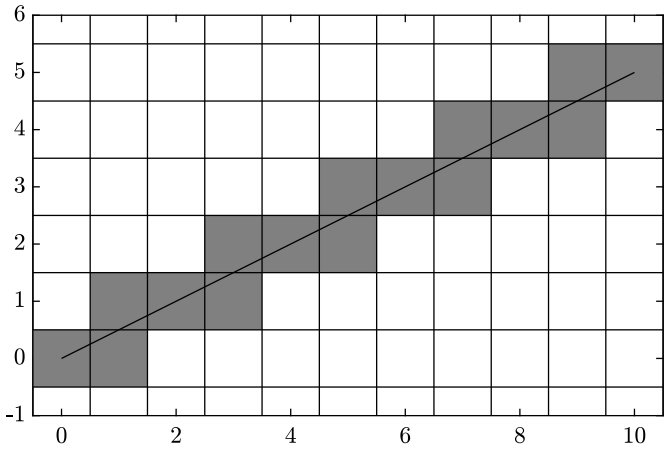

Fig. 6 discretization of a line-segment using the modified Bresenhams line algorithm

Fig. 7 shows an example result of the smoothing algorithm. It can be seen that a significant number of points have been removed, resulting in a smooth path. Also, no obstacles are touched and the transition points from one velocity region to another are preserved.

The path-finding method presented in this section was used to calculate all shortest flight paths between for all pairs of POIs given in the mission. The paths were stored for later mission generation.

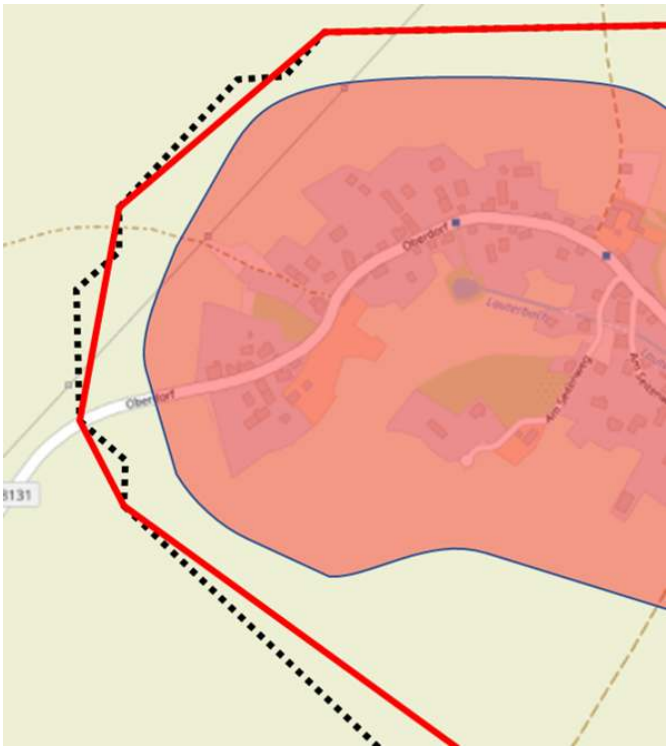

Fig. 7 Example of the post-smoothed A-Star path-finding algorithm

4 Take-off areas for Efficient Mission Routing

In this section, we address the task of selecting optimal take-off and landing areas, henceforth called "depots", to efficiently cover all locations while minimizing the overall distance traveled. Leveraging the shortest paths between all POI's in the previous section, we formulate a mixed-integer linear optimization problem aimed at strategically placing depots to enhance mission efficiency.

To identify possible depots, the (effective) length of each path between two POIs is converted into a distance matrix $D \in \mathbb{R}^{+N \times N}$:

$$D_{ij} = \text{length of path between } p_i \text{ and } p_j \tag{5}$$

The procedure to identify suitable depots consists of 3 steps:

1) Calculate the minimum number of depots needed to cover all POIs.
2) Select the optimal depots to cover all POIs, while minimizing the sum of all distances between these POIs and depots.
3) Assign each POI to exactly one depot, minimizing the total distance

Minimum number of depots needed

Define the Solution vector $x \in \{0, 1\}^N$ with N being the number of POIs, such that:

$$x_i = \begin{cases} 1, & \text{if POI}_i \text{ is selected as a depot} \\ 0, & \text{otherwise} \end{cases} \tag{6}$$

To find the minimum number n_d of depots needed, to cover all locations, a mixed-integer linear optimization problem formulated:

$$\min_x n_d = \sum_i x_i \tag{7}$$

Subject to

$$Ax \geq 1 \tag{8}$$

$$x \in \{0,1\}^N \tag{9}$$

where

$$A_{i,j} = \begin{cases} 1, & \text{if } D_{i,j} \leq \frac{R}{2} \\ 0, & \text{otherwise} \end{cases} \tag{10}$$

The parameter R in Eq. 10 describes the effective range of the UAVs. The range is restricted to half of R because the UAVs must take off and land at the same location.

Selection of optimal depots

Given the minimum number of depots $n_d \in \mathbb{N}$ found in the previous step, we can now find the optimal depots to cover all locations, while minimizing the sum of all distances between the POIs and the depots. We define the solution vector $x \in \{0,1\}^N$ similar to Eq. 6. The mixed-integer linear optimization problem to find the optimal depots is defined by:

$$\min_x f(x) = \sum_i d_i^* x_i \tag{11}$$

Subject to

$$Ax \geq 1 \tag{12}$$

$$\sum_i x_i = n_d \tag{13}$$

$$x \in \{0,1\}^N \tag{14}$$

where

$$A_{i,j} = \begin{cases} 1, & \text{if } D_{i,j} \leq \frac{R}{2} \\ 0, & \text{otherwise} \end{cases} \tag{15}$$

The term d_i^* in Eq. 11 is the sum of all distances between locations p_j the range of a possible depot p_i:

$$d_i^* = \sum_j A_{i,j} D_{i,j} \tag{16}$$

The equation 13 ensures that the number of locations selected as depots is equal to n_d, which is found in Sec. 4. The cost function (Eq. 11) penalizes the selection of depots that would result in potentially large flight missions.

Assignment of POIs to a depot

In the previous step we identified n_d optimal depots, but there are still many cases where a POI is reachable from more than one depot. Consider the solution vector $x \in \{0.1\}^{n_d \times N}$:

$$x_{mn} = \begin{cases} 1, & \text{if POI } n \text{ is assigned to Depot } m \\ 0, & \text{otherwise} \end{cases} \tag{17}$$

where n_d is the number of depots found in Sec. 4 and N is the number of POIs. To assign the POIs to exactly one depot, we can define a constraint to assign each location to exactly one depot:

$$\sum_{m=1}^{n_d} x_{mn} = 1 \; \forall \; n \in \{1, ..., N\} \tag{18}$$

The objective function is defined as follows:

$$\min \sum_{n=1}^{N} \sum_{m=1}^{n_d} x_{mn} \cdot D'_{mn} \tag{19}$$

where D'_{mn} is the distance of the shortest path between location n and depot m.

5 Mission Routing

The objective of mission routing is to optimize the utilization of flight time for each drone. This optimization is crucial for two main reasons: Firstly, manual intervention such as pre-flight checks is required for takeoff and landing, and secondly, the drones operate on fixed battery capacities. Maximizing effective flight time reduces the number of necessary turnarounds, thus minimizing overall mission duration. This optimization involves determining energy-efficient routes between Points of Interest (POIs) identified using the method outlined in Section 3. This problem falls within the domain of the Vehicle Routing Problem (VRP) [16], a generalized version of the well-known Traveling Salesman Problem (TSP) [17]. In the VRP formulation, POIs serve as nodes, and the energy consumption estimates for the shortest paths between them, derived from the method described in Section 3, determine the edge costs. Additionally, a range constraint is imposed based on the maximum effective flight range of the UAVs.

The optimization task of vehicle routing is to find the best flight missions for a fleet of UAVs visiting all POIs. In our case, "best" means that the total time to fly all missions of a depot is minimized. The total time is the sum of all flight times and the turnaround time before and after each flight. The turnaround time consists of mission preparation time, UAV inspection time, and possibly battery charging time. Therefore, our approach was to minimize the number of flights in order to minimize the turnaround time and thus maximize the use of the available battery charge per flight. The VRP is solved using OR-Tools [18], an open source software suite for solving VRP optimization problems.

The mathematical model for the used vehicle routing problem is given by:

Sets and Parameters:

- $V = \{0, 1, 2, \ldots, n\}$: Set of vertices where 0 represents the depot and $1, 2, \ldots, n$ represent customers or other locations.
- $A = \{(i, j) : i, j \in V, i \neq j\}$: Set of arcs representing possible transitions from vertex i to vertex j.
- c_{ij}: Cost of traveling from vertex i to vertex j, derived from the local distance matrix.
- Q: Maximum mission length.
- K: Maximum number of missions.

Decision Variables:

$$x_{ij}^k = \begin{cases} 1 & \text{if mission } k \text{ includes transition from } i \text{ to } j \\ 0 & \text{otherwise} \end{cases} \tag{20}$$

$$s_k = \begin{cases} 1 & \text{if mission } k \text{ is used} \\ 0 & \text{otherwise} \end{cases} \tag{21}$$

Objective Function:

$$\min \sum_{k=1}^{K} \sum_{(i,j)\in A} c_{ij} x_{ij}^k \tag{22}$$

Constraints:

1) **Coverage Constraints:** Each POI must be visited exactly once by exactly one mission to achieve full coverage.

$$\sum_{k=1}^{K} \sum_{j\in V:(i,j)\in A} x_{ij}^k = 1 \quad \forall i \in V \setminus \{0\} \tag{23}$$

$$\sum_{k=1}^{K} \sum_{i\in V:(i,j)\in A} x_{ij}^k = 1 \quad \forall i \in V \setminus \{0\} \tag{24}$$

2) **Mission Used Constraints:** Missions can only contain transitions if they are selected.

$$\frac{1}{n} \sum_{(i,j)\in A} x_{ij}^k \leq s^k \quad \forall k \tag{25}$$

3) **Depot Constraints:** Every selected mission must include the depot.

$$\sum_{j\in V:(i,j)\in A} x_{0j}^k = s^k \quad \forall k \tag{26}$$

$$\sum_{i\in V:(i,j)\in A} x_{i0}^k = s^k \quad \forall k \tag{27}$$

4) **Distance Constraints:** The sum of all transition costs in a mission must not exceed the maximum mission length.

$$\sum_{(i,j)\in A} c_{ij} x_{ij}^k \leq Q \quad \forall k \tag{28}$$

Figure 8 shows the result of the mission routing of an example depot with 14 POIs (cyan). The start and landing point is shown in magenta. Four missions are generated for this depot. Table 1 shows the most important properties of the flight mission for this depot.

The resulting individual flight missions indicate a good use of the available battery capacity. Only mission no. 1 has a low battery consumption. In addition, mission no. 1 seems to have a high energy consumption per distance traveled, considering that only one POI is visited in this flight. This is because a large part of the flight mission passes through the yellow and red zones, which require low inertial velocity limits and therefore high energy consumption.

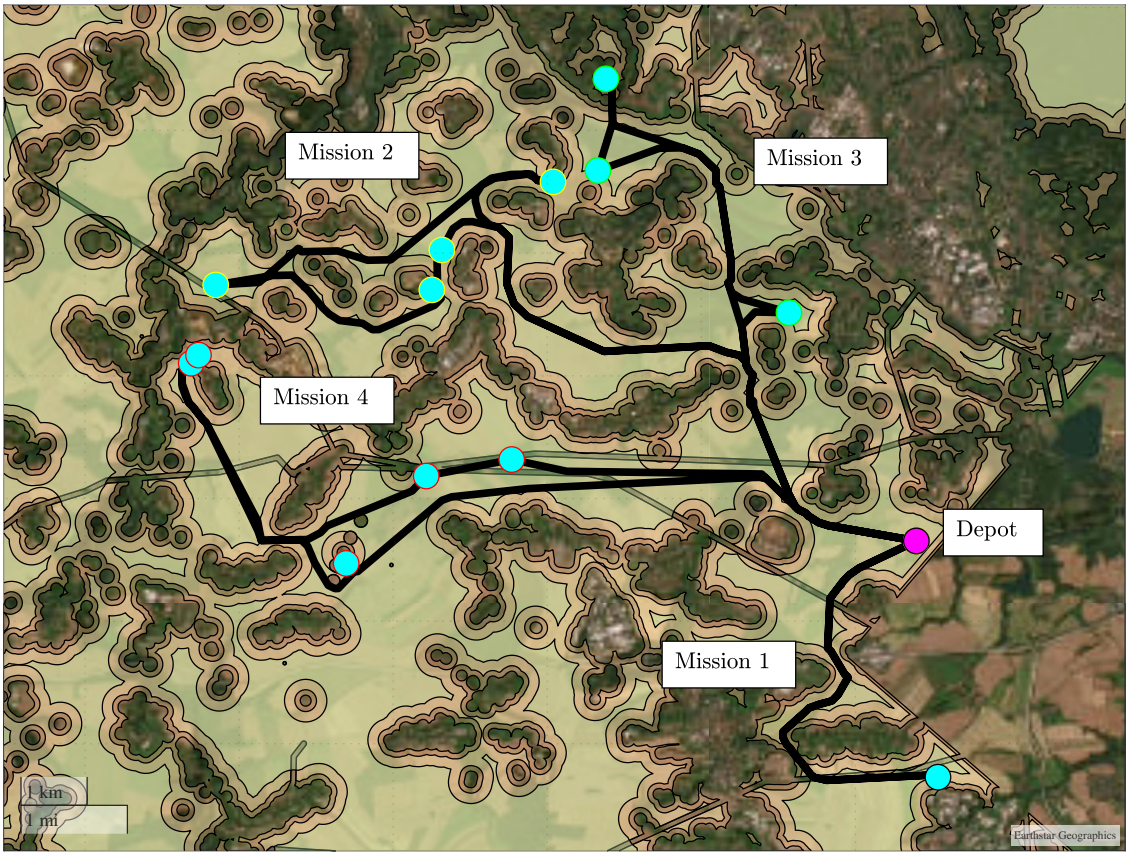

Fig. 8 Generated Missions for a depot with 14 POIs

Table 1 Details of the depot shown in Fig. 8

Mission	Flight Time [min]	Length [m]	Energy Consumption [%]
1	32	13996	62.3
2	42	28500	86.6
3	37	21694	98.5
4	45	32357	85.8

6 Results

The mission generation methodology presented in this paper was applied to a real flight campaign in Saxony, Germany. The mission consisted of 3000 POIs. Figure. 10 shows the result of the mission generation procedure. The depots are shown as bold black dots and the POIs as smaller gray dots. Similarly colored routes belong to the same depot.

A total of 494 flight missions were generated. The 3000 POIs were completely covered by 115 depots. 63 depots had less than 5 POIs assigned because the flight geography formed is-

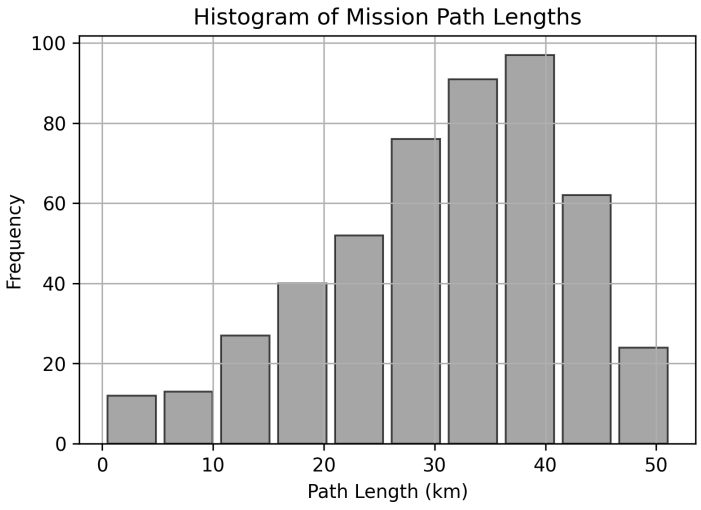

Fig. 9 Mission path lengths

lands surrounded by no-fly zones around these depots. The remaining 52 depots had an average of 55 POIs assigned. Depot 101 had 252 POIs assigned and was the largest depot.

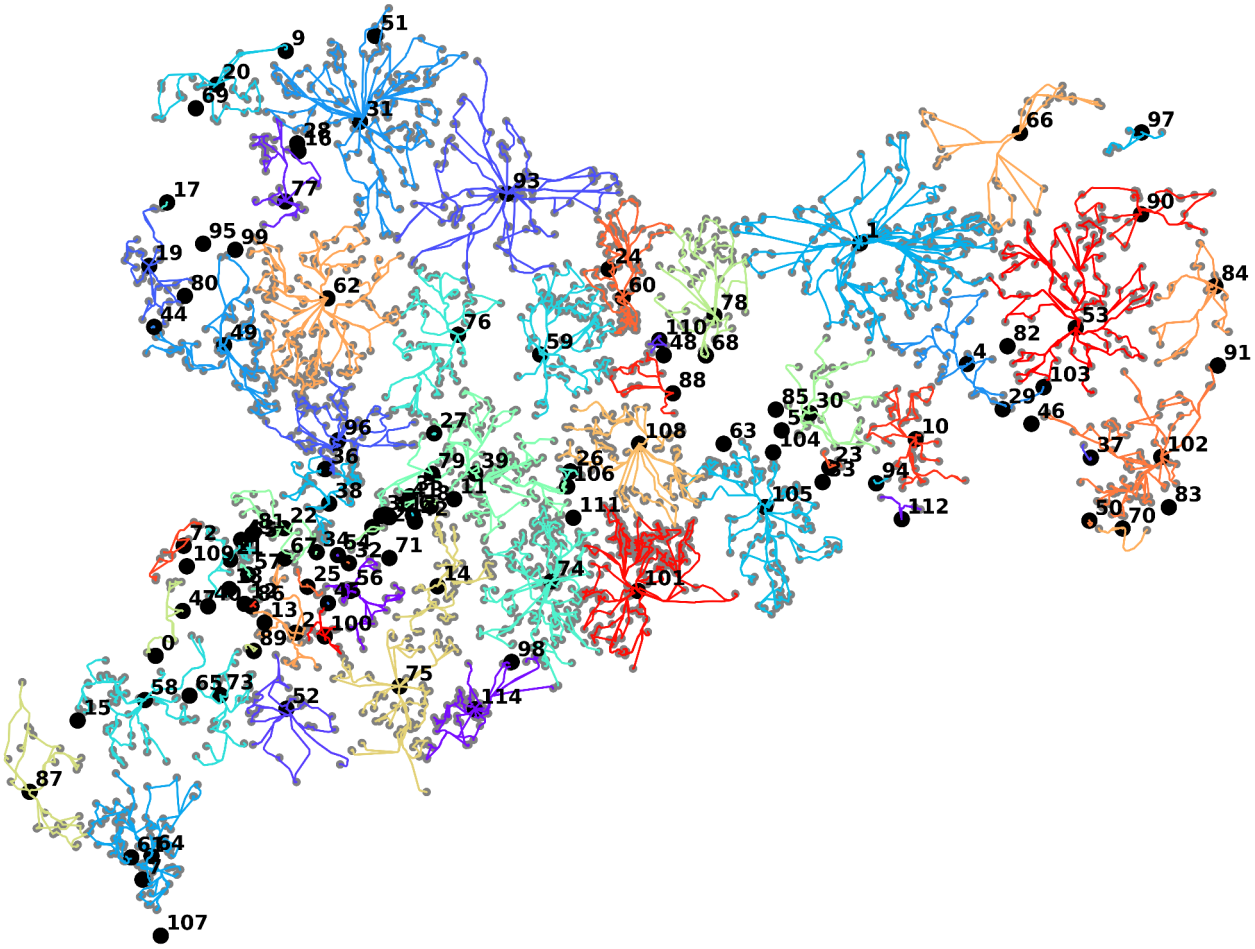

Fig. 10 Result of the mission generation procedure

The average number of flights required to complete each depot was 9, while the largest depot (101) required 20 individual flights to visit all 252 POIs. Flight missions had an average flight duration of 40 minutes and an average flight distance of 60 km.

To illustrate the effectiveness of our mission routing strategy, Fig. 9 presents the distribution of path lengths for all flight missions generated during the campaign. This visualization aids in understanding the variation in mission lengths, highlighting the efficiency of our path planning and optimization processes. By analyzing these path lengths, we can evaluate the balance between mission coverage and the constraints posed by UAV operational capacities. Table 2 shows a summary of the mission generation for the flight campaign in Saxony.

Table 2 Summary of the flight missions

Property	Mean	Max	Min
POIs per depot	26	252	5
Flights per depot	5	35	1
Fligh time in h per depot	4	30,8	2

7 Conclusion

In this paper, we present a flight path and mission generation procedure that can be used for automated aerial photography documentation of agricultural fields. The proposed methodology was applied in a large-scale BVLOS flight campaign conducted in Saxony, Germany.

The methodology incorporates a post-smoothed A-Star path-finding algorithm that enables efficient flight path generation while taking into account varying velocity constraints, obstacles such as wind turbines or power lines, and no-fly zones. Building on the path-finding algorithm, an optimization problem was formulated to identify optimal locations that serve as efficient take-off and landing points. These locations were "optimal" in the sense that they minimized the number of locations required and maximized the number of points of interest that could be reached.

In future work, we plan to extend the proposed methodology by incorporating terrain height profiles into the path-finding algorithm. The integration of terrain data will provide a more accurate representation of the flight geography, allowing for a better estimation of the battery charge or energy required to traverse specific paths. This refinement will be crucial for further optimization of automated mission routing, especially in regions with significant varying topography. In addition, the next phase of development will address the transitions between different segments of the flight path. By carefully considering the transitions from one path to another, we aim to improve the overall energy efficiency of flight missions. This comprehensive approach aims to provide a more realistic assessment of battery requirements throughout the mission routing.

Acknowledgments

We would like to extend our sincere thanks to flyXdrive GmbH for their cooperation during the Saxony Flight Campaign, which contributed to the success of our BVLOS drone flight campaign. We would also like to thank the Saxon State Ministry for Energy, Climate Protection, Environment and Agriculture and GAF AG for their invaluable support in analysing and publishing the flight campaign results.

References

[1] Javad Shahmoradi, Elaheh Talebi, Pedram Roghanchi, and Mostafa Hassanalian. A comprehensive review of applications of drone technology in the mining industry. *Drones*, 4(3), 2020. DOI: 10.3390/drones4030034.

[2] Sharifah Mastura Syed Mohd Daud, Mohd Yusmiaidil Putera Mohd Yusof, Chong Chin Heo, Lay See Khoo, Mansharan Kaur Chainchel Singh, Mohd Shah Mahmood, and Hapizah Nawawi. Applications of drone in disaster management: A scoping review. *Science & Justice*, 62(1), 2022. DOI: 10.1016/j.scijus.2021.11.002.

[3] Evan Ackerman and Eliza Strickland. Medical delivery drones take flight in east africa. *IEEE Spectrum*, 55(1), 2018. DOI: 10.1109/MSPEC.2018.8241731.

[4] Christian Eschmann. *Nahfeldnavigation unbemannter Flugsysteme zur Inspektion von Infrastrukturen*. Dissertation, 2016.

[5] Matúš Tkáč and Peter Mésároš. Utilizing drone technology in the civil engineering. *Selected Scientific Papers - Journal of Civil Engineering*, 14(1), 2019. DOI: 10.1515/sspjce-2019-0003.

[6] Elena Politi, Ilias E Panagiotopoulos, Iraklis Varlamis, and George Dimitrakopoulos. A survey of uas technologies to enable beyond visual line of sight (bvlos) operations. pages 505–512, 2021.

[7] Elena Politi, Iraklis Varlamis, Konstantinos Tserpes, Morten Larsen, and George Dimitrakopoulos. The future of safe bvlos drone operations with respect to system and service engineering. pages 133–140, 2022.

[8] Johanna Holsten, Dagmar Huth, Tobias Islam, Norbert Siepenkötter, and Dieter Moormann. Highly automated bvlos drone operations: A large scale flight campaign for agricultural observation in saxony, germany. In *Proceedings of the 2024 CEAS Specialist Conference on Guidance, Navigation and Control (EuroGNC)*, Bristol, UK, June 2024.

[9] Elena Politi, Panagiotis Rodosthenous, Ricardo J Dos Reis, Morten Larsen, Iraklis Varlamis, and George Dimitrakopoulos. Analysis of the new market trends of uavs for safe bvlos operations. 2716(1):012056, 2024.

[10] Yavor Dobrev, Nicolai Voget, Johannes Krimphove, Lennart Danielmeier, Sebastian Seitz, Johanna Holsten, and Dieter Moormann. A flight operation strategy for highly automated parallel bvlos operations. In *Proceedings of the 2024 CEAS Specialist Conference on Guidance, Navigation and Control (EuroGNC)*, Bristol, UK, June 2024.

[11] Max Hartmann, Nicolai Voget, Sebastian Seitz, and Dieter Moormann. Trajectory planning for efficient bvlos drone flights over agricultural points of interest. In *Proceedings of the 2024 CEAS Specialist Conference on Guidance, Navigation and Control (EuroGNC)*, Bristol, UK, June 2024.

[12] Fabian Baader, Ann-Kristin Sturm, Philipp Müller, Johanna Holsten, and Dieter Moormann. Operational permit: Application for flexible flight operations in the eu-2019/947 specific category. In *Proceedings of the 2024 CEAS Specialist Conference on Guidance, Navigation and Control (EuroGNC)*, Bristol, UK, June 2024.

[13] Peter E. Hart, Nils J. Nilsson, and Bertram Raphael. A formal basis for the heuristic determination of minimum cost paths. *IEEE Transactions on Systems Science and Cybernetics*, 4(2), 1968. DOI: 10.1109/TSSC.1968.300136.

[14] J. E. Bresenham. Algorithm for computer control of a digital plotter. *IBM Systems Journal*, 4(1), 1965. DOI: 10.1147/sj.41.0025.

[15] Eugen Dedu. Bresenham-based supercover line algorithm. `http://eugen.dedu.free.fr/projects/bresenham/`.

[16] Paolo Toth and Daniele Vigo. *The vehicle routing problem*. SIAM, 2002. DOI: 10.1137/1.9780898718515.

[17] W. Domschke and A. Drexl. Logistik teil: 2 rundreisen und touren, 4. *München ua*, 1997. DOI: 10.1524/9783486709971.

[18] Laurent Perron and Vincent Furnon. Or-tools. `https://developers.google.com/optimization/`.